The Astronomical Journal, 152:27 (8pp), 2016 July doi:10.3847/0004-6256/152/1/27

THE NEW ECLIPSING CV MASTER OTJ192328.22+612413.5—A POSSIBLE SW SEXTANTIS STAR

M. R. Kennedy[1,2], P. Callanan[1], P. M. Garnavich[2], P. Szkody[3], S. Bouanane[1], B. M. Rose[2], P. Bendjoya[4], L. Abe[4], J. P. Rivet[4], and O. Suarez[4]
[1] Department of Physics, University College Cork, Cork, Ireland; markkennedy@umail.ucc.ie
[2] Department of Physics, University of Notre Dame, Notre Dame, IN 46556, USA
[3] Department of Astronomy, University of Washington, Seattle, WA, USA
[4] Laboratoire Lagrange UMR 7293, Université de Nice Sophia-Antipolis, Observatoire de la Côte d'Azur, France
Received 2015 May 11; accepted 2016 April 19; published 2016 July 5

ABSTRACT

We present optical photometry and spectroscopy of the new eclipsing cataclysmic variable MASTER OTJ192328.22+612413.5, discovered by the MASTER team. We find the orbital period to be $P = 0.16764612(5)$ day/4.023507(1) hr. The depth of the eclipse (2.9 ± 0.1 mag) suggests that the system is nearly edge on, and modeling of the system confirms the inclination to be between 81°.3 and 83°.6. The brightness outside the eclipse varies between observations, with a change of 1.6 ± 0.1 mag. Spectroscopy reveals double-peaked Balmer emission lines. By using spectral features matching a late M-type companion, we bound the distance to be 750 ± 250 pc, depending on the companion's spectral type. The source displays 2 mag brightness changes on timescales of days. The amplitude of these changes, along with the spectrum at the faint state, suggest that the system is possibly a dwarf nova. The lack of any high-excitation He II lines suggests that this system is not magnetically dominated. The light curve in both quiescence and outburst resembles that of Lanning 386, implying MASTER OTJ192328.22+612413.5 is a possible cross between a dwarf nova and a SW Sextantis star.

Key words: binaries: eclipsing – binaries: general – novae, cataclysmic variables – stars: dwarf novae

1. INTRODUCTION

Binary systems in which a main-sequence or quasi-main-sequence star transfers material onto the surface of a white dwarf (WD; the primary star) are known as cataclysmic variables (CVs). There are two main categories for CVs: strongly magnetic and weakly magnetic systems. In systems containing a WD with a weak magnetic field, the material lost by the secondary leaves the L1 point to stream toward the WD and forms an accretion disk around the WD. Once the disk is formed, the stream strikes it and forms a bright (or hot) spot. The disk can extend down to the surface of the WD, and the material accretes onto the WD. In magnetic CVs, the gas stream leaving the L1 point follows the magnetic field lines to the WD and forms an accretion column for WDs with strong magnetic fields (also known as polar systems), or else for WDs with moderate magnetic fields (known as intermediate polars, or IPs), the material forms a disk until the magnetic pressure overcomes the ram pressure, in which case the disk truncates and the material flows to the WD in an accretion curtain. CVs have several photometric classifications depending on the light curves of their outbursts: classical novae have one observed large amplitude ($\Delta m > 6$) outburst; dwarf novae typically have repeated, smaller amplitude ($2 < \Delta m < 6$) outbursts; and nova-likes have no observed outbursts, but sometimes transition between high and low states of accretion (Warner 1995).

SW Sextantis stars are a subclass of high accretion rate CVs. Their defining features are: (1) they are nova-like CVs, with an orbital period $3 < P < 4$ hr; (2) they show He II λ4686 emission with a strength of half Hβ or larger; (3) the radial velocities of the emission lines vary periodically, with the Balmer lines lagging behind the expected phase for a WD based on the eclipse; and (4) absorption lines are only visible for a part of the orbit opposite the eclipse phase (Thorstensen et al. 1991). The emission lines of SW Sextantis stars are also single-peaked lines, making candidates easy to identify. The single-peaked emission lines are thought to originate from material encountering a magnetic accretion curtain close to the surface of the WD (Hoard et al. 2003). SW Sextantis stars are now thought to be the dominant population of CVs with periods between 3 and 4 hr (Rodríguez-Gil et al. 2007). Several SW Sextantis stars show circular polarization, indicative of a magnetic nature (Rodríguez-Gil et al. 2001).

Lanning 386 is an eclipsing CV with a period of 3.94 hr which defies easy classification (Brady et al. 2008). The system displays recurring outbursts with an amplitude of $\Delta m \approx 2$, but is at quiescence most of the time. This would lead Lanning 386 to be classified as a dwarf nova. The spectrum of Lanning 386 in quiescence is consistent with this classification, but the spectrum in outburst tells another story. The spectrum in quiescence shows single-peaked Balmer emission lines, and in outburst displays strong, single-peaked He I and He II lines, and the strong excitation C IV line, consistent with a SW Sextantis star (Groot 2000). However, in quiescence and outburst, Lanning 386 does not show the emission line radial velocity phase lag expected of the SW Sextantis stars (Brady et al. 2008). Also of interest is the recurrence time of the outbursts, which is only a few days. Other scenarios have been considered, such as Lanning 386 being a VY Scl system (which are nova-like, non-magnetic or weakly magnetic CVs which exhibit low states on a recurrence time of years (Leach et al. 1999)) or even an IP, but again, Lanning 386 only shares some of the characteristic features of these classes, never all. Its true classification still remains a mystery, but it is currently best described as a dwarf nova in quiescence and a SW Sextantis star in outburst.

MASTER OTJ192328.22+612413.5 (hereafter referred to as J1923 and shown in Figure 1), the subject of this paper, was initially discovered by the MASTER-Tunka auto-detection system in April 2014 (Balanutsa 2014). The magnitude of J1923 was observed to be 19.2 in 2010, but had brightened to

an unfiltered magnitude of 17.5 on 2014 April 20 and 17.7 on 2014 April 22. It was classified as a CV due to its 2 mag difference with respect to reference images. There is also a UV counterpart to J1923, GALEX J192328.3+612413, which has a far-UV (FUV) magnitude of 19.42 ± 0.15 and near-UV (NUV) of 19.68 ± 0.10, obtained on 2007 June 1. J1923 was also detected in the infared as WISE J192328.25+612413.1. The ALLWISE Source Catalog lists magnitudes of W1 = 16.58 ± 0.05 and W2 = 16.6 ± 0.1 for J192328.25 +612413.1. It was also suggested that J1923 might be a magnetically dominated CV, or polar, due to its proximity to the *ROSAT* X-ray source 1 RXS J192333.2+612507, which has a large error circle of 14″.

In this paper, we present photometry and spectroscopy of the newly discovered CV J1923, and use the data to obtain a period for the system and classify its CV type. We also estimate the inclination of the system based on analysis of the depth of the eclipse. Finally, we present a distance estimate using constraints on the companion spectral type.

2. OBSERVATIONS

2.1. Photometry

Photometry of J1923 was taken in the SDSS g band using the 1.8 m Vatican Advanced Technology Telescope (VATT) located at Mount Graham International Observatory over four consecutive nights, starting 2014 April 29 (UT). The images were taken using the VATT4K CCD with a typical exposure time of 30 s. A total of 880 images were taken over these four nights. There are deep eclipses visible on the third and fourth nights of the run. On the first night, there is an eclipse that is not well determined due to the onset of twilight.

A single night of V-band photometry was acquired at the VATT on the night of 2014 June 28 (UT). A total of 518 images were taken with a typical exposure time of 15 s. There is a clear eclipse visible in these data.

Data were also acquired from the dual 1 m telescopes C2PU facility at the Calern Observatory (Observatoire de la Côte d'Azur, France) in the second half of 2014 August. A total of 245 40 s exposures with no filter, 100 60 s exposures with no filter, and 83 simultaneous 60 s exposures using V and R filters were obtained. There are eclipses visible in all of these data sets.

2.2. Spectroscopy

Spectroscopy of J1923 was taken using the Dual Imaging Spectrograph on the 3.5 m ARC telescope at Apache Point Observatory on the night of 2014 June 21 (UT). The blue channel used the B1200 grating, which has a pixel scale of 0.62 Å pix^{-1}, while the red channel used the R1200 grating, which has a pixel scale of 0.58 Å pix^{-1}. A total of five 900 s long exposures were obtained on the blue and red channels. The first three spectra were obtained at an airmass greater than 1.4, while the final two spectra were taken later in the night, at an airmass of 1.2.

Figure 2 shows the average spectrum for J1923, with variations due to the orbital motion of the system unaccounted for. The average spectrum shows distinct double-peaked emission lines, corresponding to Hα, Hβ and Hγ lines, along with a rise toward the red end of the spectrum. The flux of J1923 in the V-band section of the spectrum in Figure 2 is $\approx 0.45 \times 10^{-16}$ erg cm^{-2} s^{-1} Å^{-1}. This corresponds to a V-band magnitude of 19.8, which is the magnitude of J1923 in the low state.

3. RESULTS

The light curves for each night after standard photometric calibration can be seen in Figure 3. All data reduction and photometry was performed using standard IRAF[5] tasks. Photometry was carried out on J1923 using the PHOT command from the DIGIPHOT package, and the images were calibrated using nearby stars from the Sloan Digital Sky Survey (SDSS) catalog.

3.1. Period and Ephemeris

The period of the system was found by applying a phase dispersion minimization (PDM; Stellingwerf 1978) to the data, which were first normalized to have a common non-eclipse magnitude. The period range was set to between 0.15 and 0.2 day. The resulting theta plot can be seen in Figure 4. The best-fit period is 0.16765 ± 0.00004 day, with the error being the width of this peak. The periods on either side of the deepest trough were tested, and were found to give poor fits.

The time of the midpoint of each observed eclipse was found by fitting a Gaussian to the eclipse profiles (see Figure 5 for an example), and using the center of the Gaussian as the time of mid-eclipse, with the error in the time being the error in fitting the center of the Gaussian. These times and the associated eclipse numbers can be seen in Table 1, where the eclipse number was found by taking the third night's eclipse as 0, and using the newly discovered period to find the remaining eclipse numbers relative to this night. The first night's eclipse has a much higher error than other nights as the eclipse was only partially observed. For this night, a model eclipse was constructed using a Gaussian, and the midpoint adjusted manually to see where the Gaussian matched the beginning of the eclipse.

A linear fit was applied to the data, and the resulting ephemeris was

$$T_{\rm mid}\,({\rm HJD}) = 2456778.83690(3) + 0.16764612(5)E. \quad (1)$$

The phased light curve using the linear ephemeris can be seen in Figure 6.

3.2. Light Curve Morphology

The first two nights of observations show a light curve with a pre-eclipse hump starting at phase 0.7, along with quasi-periodic oscillations (QPOs) just after the eclipse. The data were masked to remove the eclipses, and then each night of data was subjected to a Lomb–Scargle periodogram (Lomb 1976; Scargle 1982). The power spectra for each night were then multiplied together to reduce the power of the noise peaks while maintaining power in the peaks common to each data set. The resulting power spectrum can be seen in the lower half of Figure 7. There are several strong peaks around a frequency of ~3.3 hr^{-1} ($P_{\rm QPO}$ ~ 20 minute). The top panel of Figure 7 shows a sine wave with a period of 21 minute plotted on top of the data from 2014 April 29, when the system was in its low state and the QPOs were most prominent. The broad

[5] IRAF is distributed by the National Optical Astronomy Observatory, which is operated by the Association of Universities for Research in Astronomy (AURA) under cooperative agreement with the National Science Foundation.

power spectrum confirms these oscillations are not coherent and cannot be solely due to the spin of the central WD. Kilosecond QPOs have been seen in SW Sextantis stars before, and are thought to arise from magnetic WDs that are drowned by a high accretion rate (Patterson et al. 2002).

The light curve also shows two distinct states. The quiescent state has a non-eclipse magnitude of 19.5 in the g band from the first two nights (frames (a) and (b) of Figure 3), and the pre-eclipse hump and QPOs are distinct. The system had an out-of-eclipse magnitude that gradually decreased from night to night as the system went into outburst. On the first night of outburst (Figure 3(c))), the average magnitude was 18.2, while on the second night of outburst, the system had brightened again to $m < 18$. The depth of the eclipse in outburst, which was well covered by observations, was $\Delta m = 3.2 \pm 0.1$ mag as seen in the g band and $\Delta m = 2.9 \pm 0.1$ in the V band.

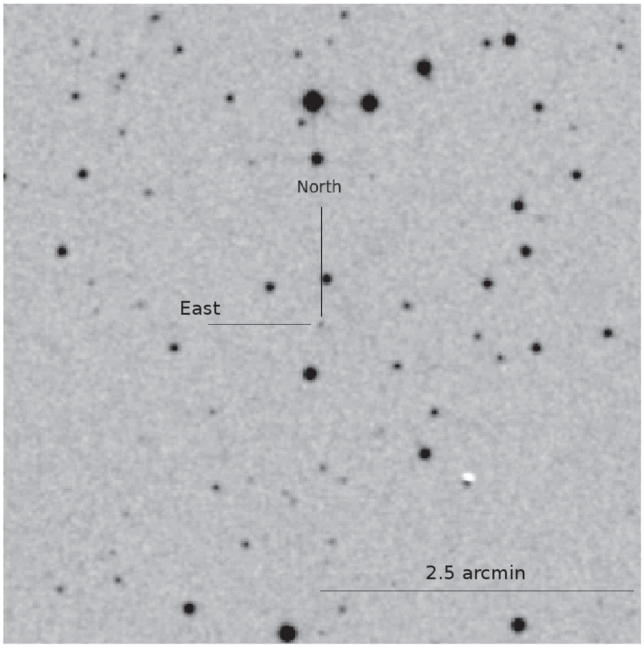

Figure 1. Finding chart for J1923+6124, taken from the STScI Digitized Sky Survey. The photometry was calibrated using the bright star just to the south of J1923, which has a g-band magnitude of 15.64, a V-band magnitude of 15.19, and an R-band magnitude of 15.13.

The eclipse width was found by fitting a Gaussian to the V-band data, after conversion from magnitude to flux. The resulting fit gave an eclipse width (FWHM) of 0.081 ± 0.001 in phase.

3.3. Emission Spectrum

By using the calculated ephemeris, we found the phase of each of the spectra obtained: 0.81, 0.87, 0.21, 0.29, and 0.35. The rise toward the red end of the spectrum is thought to be molecular bands visible from the companion star which match that of a late M-type star, similar to the companion of Lanning 386 (Brady et al. 2008). This is further discussed in Section 4.2. The equivalent width (EW) of the Hα, Hβ and Hγ lines can be seen in Table 2, along with the Balmer decrement.

The full width at zero intensity (FWZI) of Hα, Hβ, and Hγ was measured within `IRAF`, as were the peak-to-peak separations of the Hα, Hβ, and Hγ lines, found by fitting a double Lorentzian to the line region, and can be seen in Table 2. The fits gave separations of 16 Å, 16 Å, and 15 Å, respectively. The asymmetry between the blue and red peaks could be due to the presence of the hotspot.

4. DISCUSSION

4.1. Inclination and Mass Ratio of J1923

The depth of the eclipse is 3.2 ± 0.1 mag seen in the g band on nights three and four of the data and 2.9 ± 0.1 mag in the V band on night five. The majority of CVs with an eclipse depth close to or larger than 2.5 mag have an inclination angle greater than 85° (Ritter & Kolb 2003). Hence, the inclination of J1923 is expected to be >85°, suggesting that J1923 is a nearly edge on disk system.

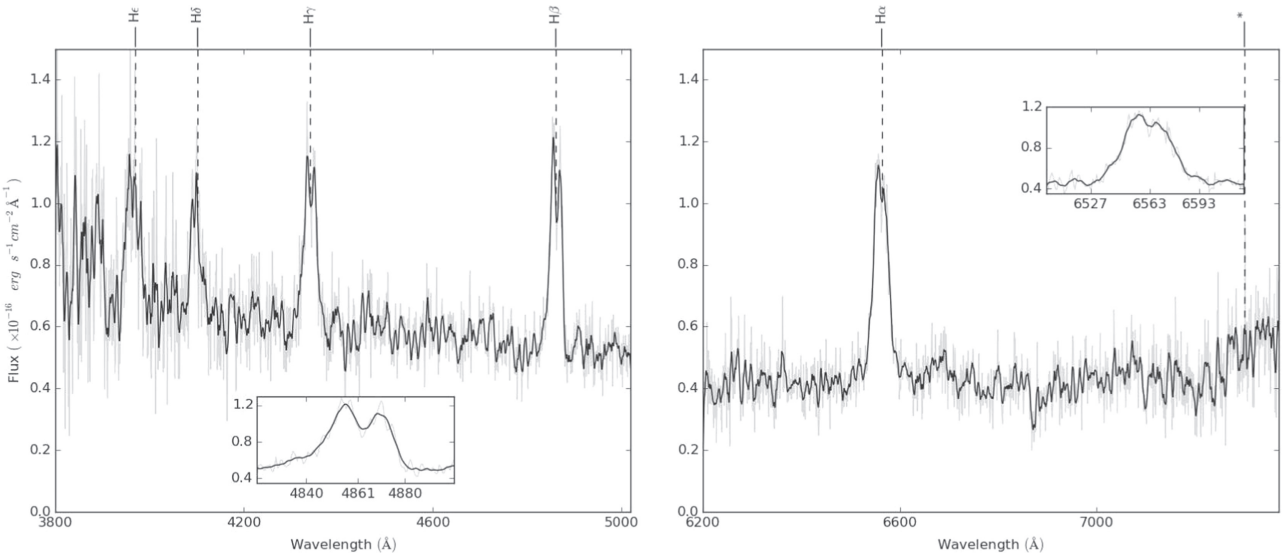

Figure 2. Average spectrum of J1923 in quiescence. The left panel shows the blue spectrum while the right panel shows the red spectrum. The spectra have been boxcar smoothed with a width of 6 Å. The gray spectrum shows the unsmoothed data. The most prominent emission features are marked. The inset on the left shows the double-peaked Hβ line, while the right inset shows the double-peaked Hα line. There is a clear rise toward the red in the spectrum on the right which is marked with a *, which matches a late M-type star. Analysis of the lines can be seen in Table 2.

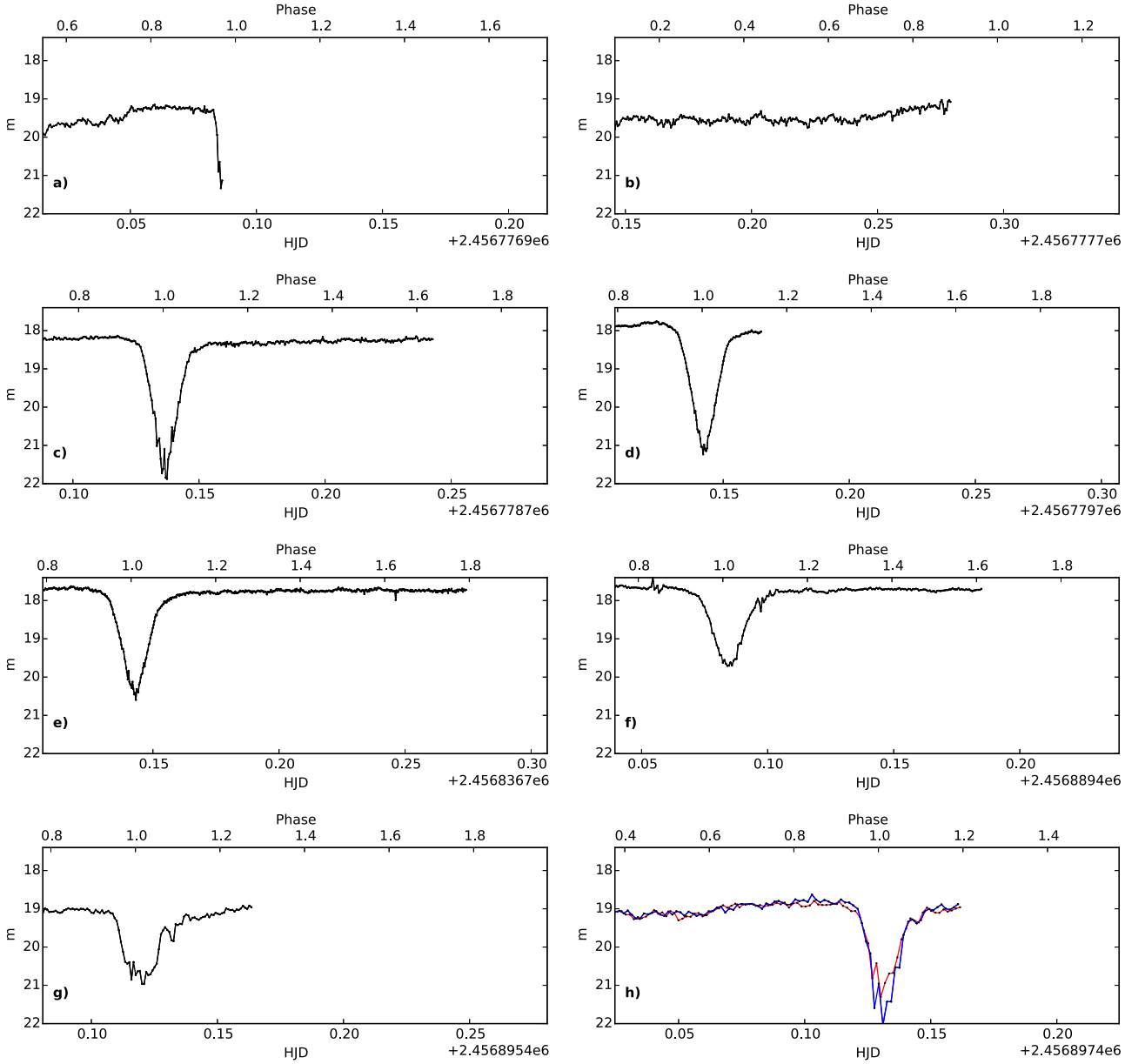

Figure 3. Light curve of J1923. Frames (a), (b), (c), and (d) were taken on sequential nights in the SDSS g band. Frames (a) and (b) show the light curve in quiescence, with the hump from the hotspot visible in frames (a) and (b), and the QPOs visible in frame (b). The system went into outburst between frames (b) and (c), with the brightness of the system again increasing between frames (c) and (d). Frame (e) was taken two months later, at the end of 2014 June, in the V band with a typical exposure time of 15 s. Frame (f) was taken two months later again, at the end of 2014 August, without a filter, and with a typical exposure time of 40 s. Frame (g) was also taken in August, with no filter and a typical exposure time of 60 s as the system was in quiescence. Frame (h) shows the simultaneous V and R filter data taken in August, with a typical exposure time of 60 s. The V-band data are displayed in blue, and the R-band data are in red.

The Hα peak-to-peak separation of 16 Å corresponds to a velocity separation of 800 km s^{-1}. This would normally limit the inclination of the system to be $<30^{\circ}$ (Horne & Marsh 1986). However, such a deep eclipse is difficult to explain with such a low inclination. Instead, it is possible that this low peak-to-peak separation is due to a truncation of the accretion disk far from the surface of the primary, which might be due to the presence of a strong magnetic field on the WD, or a low velocity component (spot or wind perpendicular to the disk or magnetic curtain) could fill-in the line center (Hoard et al. 2003).

The lower bound on the FWZI of J1923 is smaller than the FWZI of some high inclination SW Sextantis systems (Dhillon et al. 2013), which are thought to contain magnetically truncated disks (Hoard et al. 2003). This supports the idea that the accretion disk in J1923 may be truncated due to the presence of a magnetic field.

4.1.1. Modeling the Quiescent Light Curve

The light curve in quiescence was modeled using the Eclipsing Light Curve Code (ELC; Orosz & Hauschildt 2000). The basic model consisted of a WD with a temperature of 32,000 K (see Section 4.2 for more detail), an inner accretion disk radius in the range of 1–13$R_{\rm WD}$, a temperature gradient in the disk $\left(T(r) = T_i\left(\frac{r_i}{r}\right)^{\zeta}\right)$ of 0.75 (which assumes a "steady-state" disk), a hotspot with angular size in the range of

2°–4° centered on orbital phase 0.86, and an inclination between 72° and 90°. We computed best-fit models based on the χ^2 statistic using ELC for mass ratios $\left(q, = , \frac{M_{\rm sec}}{M_{\rm WD}}\right)$ of 0.5, 0.4, 0.33, 0.285, and 0.25 and for inner disk temperatures (T_d) of 15,000 K, 16,000 K, and 17,000 K. Table 3 shows the best-fit inclination and χ^2 for each model.

The resulting V-band fit to the data can be seen in Figure 8, which shows the best and worst fits of our modeling. The best-fit inclination range over all models was very narrow, between 81.°3 and 83.°6. A mass ratio of $q = 0.5$ provides the best overall fit.

The ingress of the eclipse is never well fit by any of our models, with the observed ingress always steeper than in any of our models. This is a result of the simple model ELC assumes for the hotspot. ELC simply increases the temperature of the accretion disk cells which correspond to the position of the hotspot, instead of making the hotspot an independent structure. As such, ELC is not able to include eclipsing of the accretion disk by a physical hotspot for high inclination systems, which, in reality, would steepen the ingress.

4.2. Modeling the Spectrum

We next modeled the *GALEX* FUV and NUV fluxes, along with the optical spectrum, to constrain the temperature of the WD and the contribution of the secondary star. WD model atmospheres were generated using Hubeny's TLUSTY, SYNSPEC, and ROTIN programs (Hubeny 1988; Hubeny & Lanz 1995) for WD temperatures between 24–34,000 K and with a log$g$ of 8.

Schlafly & Finkbeiner (2011) estimated the reddening in the direction of J1923 to be $E(B-V) = 0.0471 \pm 0.0015$ mag. In the following, the spectrum has been de-reddened using this value and the Cardelli extinction function (Cardelli et al. 1989), implemented in the `PYTHON` module `ASTROPYSICS`.

Table 4 shows the results of our spectral fitting. The lowest temperature WD which provided an acceptable fit to the UV and the optical was a WD with a temperature of 24,000 K and a minimum amount of disk contribution, along with a companion of spectral type M5V (the stellar spectrum was obtained from the MILES catalog (Sanchez-Blazquez et al. 2006)). This fit can be seen in Figure 9.

The best-fit model from Table 4 gives a WD temperature of 34,000 K and an accretion disk with an inner temperature of 15,000 K. However, there is a degeneracy between all of our fits, which can be seen in the small change in the reduced χ^2 between all of the models. The only limit our modeling reveals is that the lowest temperature WD which fits our data is 24,000 K, as cooler WDs cannot be fit with an accretion disk contribution.

The contribution of the secondary is similar throughout our models, with a flux between (2–2.5) $\times 10^{-16}$ erg s^{-1} cm^{-2} Å^{-1} at 5500 Å.

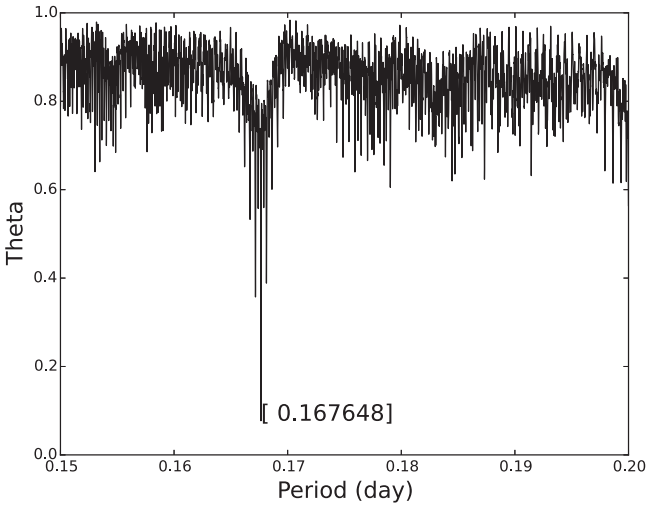

Figure 4. PDM of the light curve of J1923. The deepest minimum occurs at $P = 0.16765 \pm 0.00004$ day.

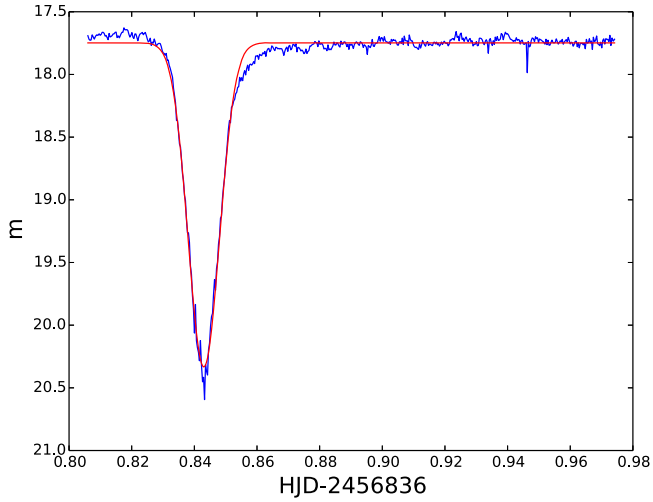

Figure 5. Eclipses were modeled using a Gaussian function to accurately determine the time of mid-eclipse. Above is a single night's data from the VATT from 2014 June, with the red line representing the best Gaussian fit.

Table 1
Summary of Observations

Frame in Figure 3	Date Observed 2014	Filter	State	Eclipse Number	Mid-eclipse Time (HJD-2,450,000.0)	Uncertainty (day)
(a)	Apr 28th	SDSS-g	Low	−11	6776.992	0.001
(b)	Apr 29th	SDSS-g	Low	N/A	⋯	⋯
(c)	Apr 30th	SDSS-g	High	0	6778.83667	0.00009
(d)	May 1st	SDSS-g	High	6	6779.84257	0.00004
(e)	Jun 27th	V	High	346	6836.84301	0.00004
(f)	Aug 19th	Clear	High	660	6889.48331	0.00001
(g)	Aug 25th	Clear	Low	696	6895.51890	0.00004
(h)	Aug 27th	V/R	Low	708	6897.53010	0.00007

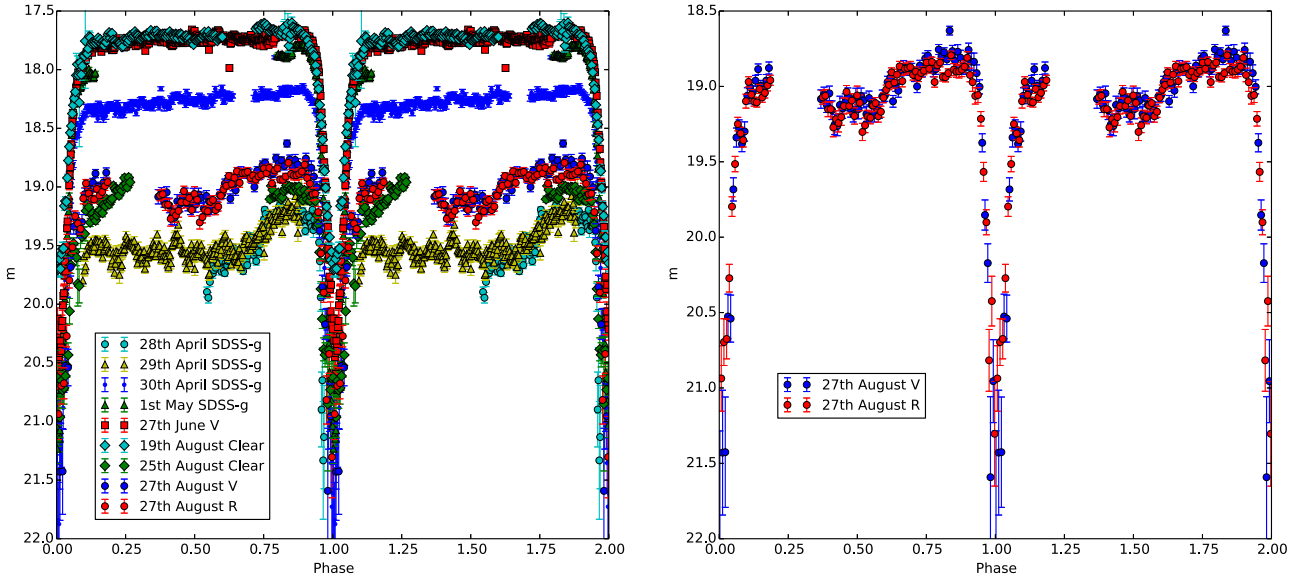

Figure 6. Left panel: the phased light curve for J1923 for all eight nights of data using the linear ephemeris. Right panel: just the simultaneous R- and V-band data taken in 2014 August.

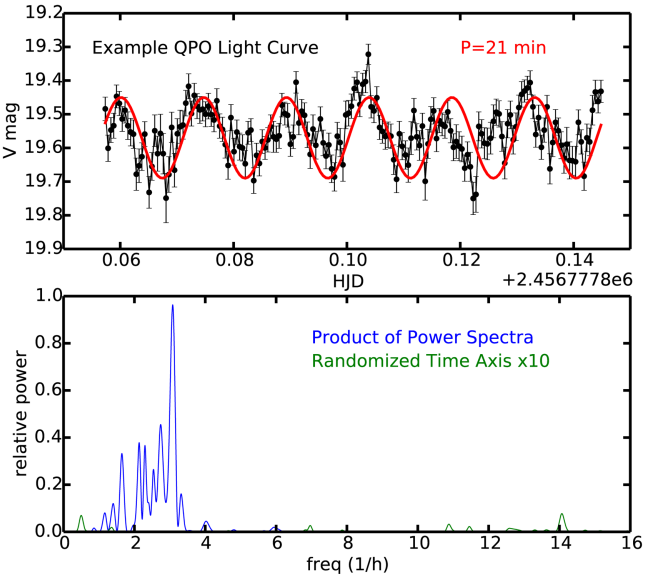

Figure 7. Bottom panel: the power spectrum of the data with the eclipses masked, in order to look for the period of the QPOs. The blue shows the power spectrum of the normal data, while the green shows the power spectrum of the data after they had been randomized, to make sure the peaks in the original power spectrum were not due to noise. Top panel: a sine wave with a frequency of 3.32 hr^{-1} plotted alongside the data from 2014 April 29, when the system was in its low state and had the most prominent QPOs.

Table 2
Properties of the Emission Lines Seen in the Average Spectrum of J1923

Feature	EW	Flux	FWZI[a]	FWHM[b]	Balmer Decrement
	Å	10^{-17} erg cm^{-2} s^{-1}	km s^{-1}	km s^{-1}	
Hα	47	217	$\gtrsim$2800	1500	1.20
Hβ	35	181	$\gtrsim$3000	1700	1
Hγ	24	146	$\gtrsim$3800	2000	0.81

Note. (a) The FWZIs are given as lower limits since the ability to determine the extension of the line wings is usually set by the signal-to-noise ratio in the data. (b) Measured using a Gaussian fit.

Table 3
The Best-fit Models Computed Using a χ^2 Grid Search with ELC for Various Mass Ratios (q) and Inner Disk Temperatures (T_d)

q	T_d(K)	i°	χ^2	χ^2_R
0.5	15000	81.4–83.2	2140	4.89
	16000	81.4–83.2	2118	4.85
	17000	81.8–83.6	2097	4.80
0.4	15000	81.4–82.8	2191	5.01
	16000	81.7–83.0	2165	4.95
	17000	81.9–83.6	2147	4.91
0.33	15000	81.8–82.8	2243	5.13
	16000	82.0–83.1	2213	5.06
	17000	82.3–83.4	2187	5.00
0.285	15000	81.3–83.0	2293	5.25
	16000	81.8–83.1	2259	5.17
	17000	82.1–83.5	2230	5.10
0.25	15000	81.5–82.9	2323	5.32
	16000	81.8–83.1	2290	5.24
	17000	82.2–83.6	2260	5.17

The V-band magnitude of our M5V template is 20.7 ± 0.3. This gives a V–W1 of 4.1 ± 0.3, assuming that the *WISE* magnitudes were taken when J1923 was in quiescence. This is much higher than the V–W1 of 6.2 for an M5V star, but is closer to the V–W1 of 5.2 for an M4V star (Pecaut & Mamajek 2013). Hence, we conclude the companion spectral type is M4–5. This spectral type is also in keeping with the results from Knigge et al. (2011), which shows that the expected spectral type for a CV with a period of 4 hr is a M4–M5. Furthermore, this spectral type is similar to the M5.5 ± 0.5 companion of HS 0220+0603, another eclipsing SW Sextantis system with an orbital period between 3 and 4 hr (Rodríguez-Gil et al. 2015).

We use the V-band magnitude of the companion in the model spectrum of 20.9 ± 0.3, along with an absolute magnitude of 12.3 for an M5 star, to compute a distance to J1923 is $d = 520 \pm 80$ parsec. If the companion is a M4 star, then using an absolute magnitude of 11.2, the distance to J1923 is $d = 900 \pm 100$ parsec.

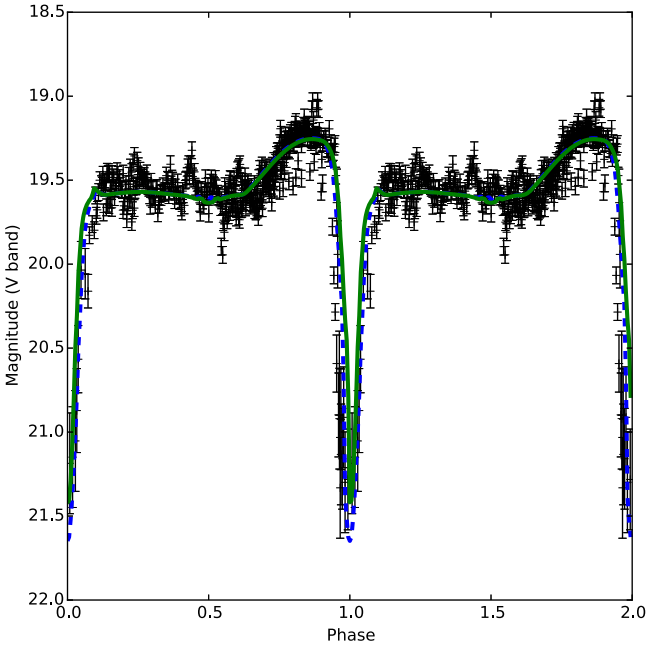

Figure 8. Best (blue dashed line; $q = 0.5$, $T_d = 17{,}000$ K, $i = 83^\circ.1$) and worst (green solid line; $q = 0.25$, $T_d = 15{,}000$ K, $i = 82^\circ.25$) model light curves generated by ELC plotted against the low state data of J1923 (black). The ingress of the eclipse is deeper in the data than in any of our models, and is possibly related to how ELC models hotspots.

Table 4
The Reduced χ^2 Values for Various Fits to the Optical Spectrum and *GALEX* Fluxes of J1923

WD Temp (K)	T_d(K)	χ^2_R
24000	15000	1.15
	16000	1.15
	17000	1.16
26000	15000	1.13
	16000	1.14
	17000	1.14
28000	15000	1.12
	16000	1.12
	17000	1.13
30000	15000	1.10
	16000	1.11
	17000	1.12
32000	15000	1.09
	16000	1.10
	17000	1.11
34000	15000	1.09
	16000	1.10
	17000	1.10

4.3. Similarity to Lanning 386

Figure 10 shows a previously unpublished light curve of Lanning 386 in quiescence, taken in 2009 using the Galway Ultra Fast Imager (GUFI) on the VATT. The calibrated V-band magnitude of Lanning 386 outside eclipse is 17.5 in quiescence. The similarities between the light curve for Lanning 386 and those presented here for J1923 are beyond coincidence. Both objects show QPOs in the quiescent state, and have visible humps at phase 0.75. Both objects lose both of these features while in outburst, and brighten by similar magnitudes.

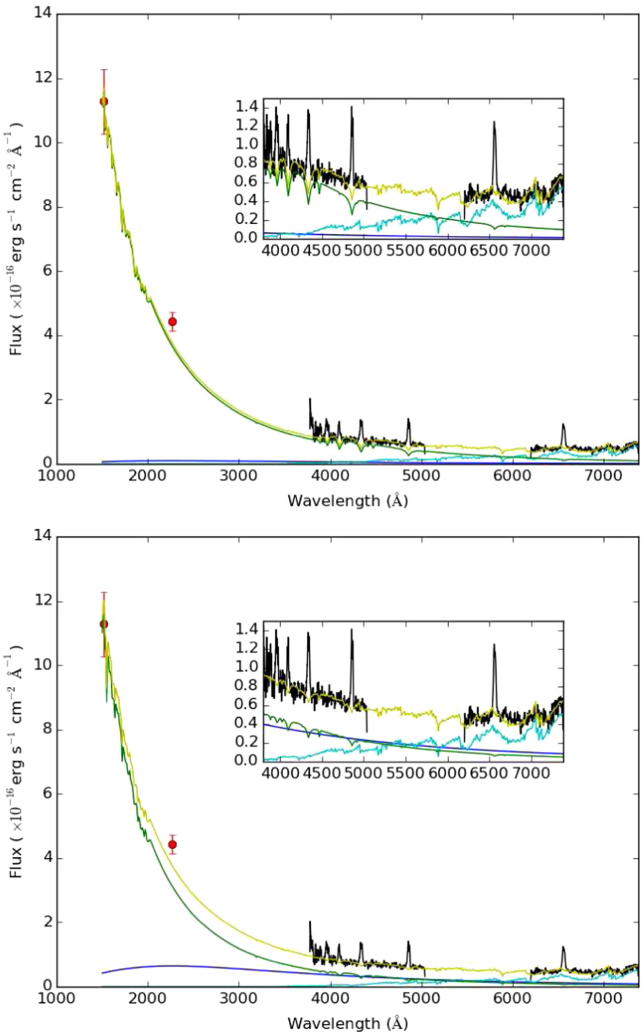

Figure 9. Top: the lowest WD temperature model spectrum fit to the *GALEX* fluxes and optical spectrum. The green curve is a WD model with $T = 24{,}000$ K and $\log g = 8$. The green curve is an accretion disk with inner temperature of 15,000 K and $\xi = 0.75$. The cyan curve is the M5V spectrum from the MILES catalog. The yellow is the sum of the three components. The inset is a zoom of the optical spectrum. Bottom: requiring an equal contribution in optical flux between an accretion disk (with a maximum temperature of 15,000 K and a $\xi = 0.75$, shown in blue) and a WD of temperature of $T = 34{,}000$ K gives a good fit to the spectrum, along with the same comparison star as in the top panel. A cooler WD allows for the WD to dominate in the optical, which is inconsistent with the results of the ELC modeling.

The spectra of both objects, taken when both were in quiescence, are also very similar. The Balmer decrements of Lanning 386 are $D_{34} = 1.15$ and $D_{54} = 0.85$ (Brady et al. 2008), which are within the measurement errors of the decrement for J1923. Both spectra also show the same M-type molecular band past 7200 Å. Lanning 386 displays two very different spectra, depending on its state. When in quiescence, its spectrum is identical to that observed here for J1923. However, in outburst, Lanning 386 displays prominent ionized helium emission lines, along with the Bowen Blend structure and C IV($\lambda = 5806$ Å). The spectrum shown in Figure 2 was taken when J1923 was in the low state, which might explain the absence of the features seen in the excited state in Lanning 386.

The peak-to-peak separation of the emission lines in J1923 is small compared to the expected value for its high inclination, and the FWZI is smaller than the value typically found in SW

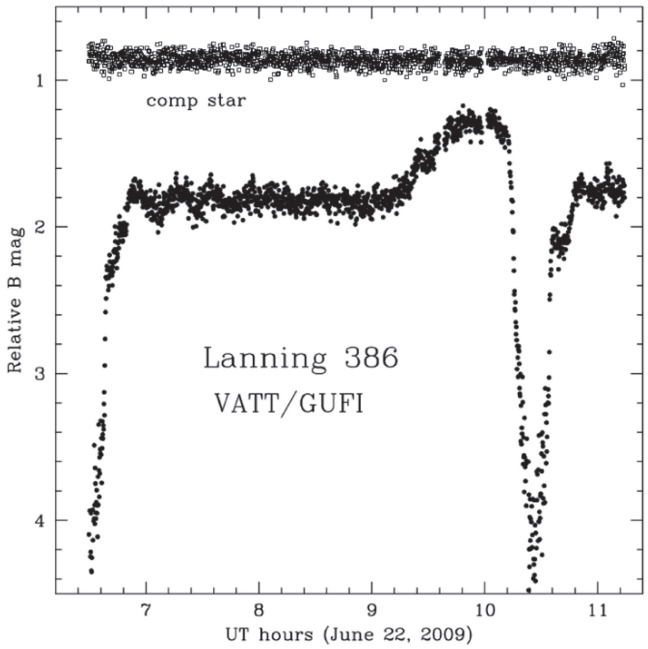

Figure 10. Previously unpublished VATT/GUFI light curve for Lanning 386, showing pre-eclipse hump and QPOs.

Sextantis stars. We propose that this is possibly due to a truncation of the accretion disk due to the WDs magnetic field.

The single-peak structure seen in SW Sextantis stars is thought to arise due to a strong magnetic accretion curtain (Hoard et al. 2003). A possible explanation for the slightly double-peaked emission lines in J1923 could also be that there is weaker line emission from the accretion curtain in J1923, as opposed to the strong emission line core seen from the magnetic accretion curtain in SW Sextantis stars.

5. CONCLUSIONS

We have found the period of J1923 to be $P = 0.16764612(5)$ day and determined a linear ephemeris for eclipses observed from 2014 April to June. The best-fit model to the eclipses requires a high inclination of $85.^{\circ}5 \pm 2^{\circ}$ and a disk which does not extend to the surface of the WD. This inclination is greater than the inclination estimated using the peak-to-peak separation of the Hα line. However, the small FWZI of the emission lines may suggest the accretion disk is truncated by the magnetic field of the WD, as proposed by Hoard et al. (2003).

J1923 shares many similarities with Lanning 386. Both show QPOs in quiescence, have similar outburst amplitudes of $\Delta m \approx 2$, have similar orbital periods and have similar Balmer line spectra in quiescence. Even though it is still debatable whether both of these systems have anything to do with the SW Sextantis stars, it is nearly certain that they are extremely similar to each other. To confirm this, more simultaneous high-resolution spectroscopy and photometry of J1923 is required to see if the He II lines become prominent when the system is in outburst. It would also be of interest to see if the C IV 5806 Å line which is visible in Lanning 386 during outburst is also present in J1923, as the C IV line is a high-excitation line rarely seen in CVs, yet has been observed in SW Sextantis, and is also present in Wolf–Rayet stars. It would also be interesting to observe J1923 in the X-ray region, as strong X-ray emission would suggest that J1923 may be a magnetic system. In that case, the accretion disk would be truncated before reaching the surface of the WD, which would help explain why the emission lines appear single-peaked, despite their inferred inclination. This scenario also requires a very weak emission component from a magnetic accretion curtain, as there is no evidence for a strong core in the emission lines of J1923. If this X-ray emission were also seen in Lanning 386, it would help explain why the emission lines seem single-peaked, despite the system's inferred inclination.

If J1923 does exhibit the He II line at 4686 Å when in outburst, then the question still remains as to what causes this emission in both J1923 and Lanning 386. The V Sagittae stars are CVs with long periods ($5 < P < 24$ hr) which display very prominent He II 4686 Å emission (Steiner & Diaz 1998). It is possible that the V Sagittae stars and SW Sextantis stars are related through stars similar to J1923 and Lanning 386, and that the He II 4686 Å emission is the key to linking these interesting classes together.

M.R.K., P.C., and P.M. acknowledge financial support from the Naughton Foundation, Science Foundation Ireland and the UCC Strategic Research Fund. P.S. acknowledges support from NSF grants AST-1008734 and AST-1514737. We thank the Vatican Observatory and Richard Boyle for providing us observing time on the VATT. Some of this work is based on observations obtained with the Apache Point Observatory 3.5 m telescope, which is owned and operated by the Astrophysical Research Consortium. We would also like to thank the anonymous referee for constructive and useful feedback.

Facilities: VATT, ARC.

REFERENCES

Balanutsa, P., Denisenko, D., Lipunov, V., et al. 2014, ATel, 2014, 6097
Brady, S., Thorstensen, J., Koppelman, M., et al. 2008, PASP, 120, 301
Cardelli, J. a., Clayton, G. C., & Mathis, J. S. 1989, ApJ, 345, 245
Dhillon, V. S., Smith, D. a., & Marsh, T. R. 2013, MNRAS, 428, 3559
Groot, P. J. 2000, NewAR, 44, 137
Hoard, D. W., Szkody, P., Froning, C. S., Long, K. S., & Knigge, C. 2003, AJ, 126, 2473
Horne, K., & Marsh, T. 1986, MNRAS, 218, 761
Hubeny, I. 1988, CoPhC, 52, 103
Hubeny, I., & Lanz, T. 1995, ApJ, 439, 875
Knigge, C., Baraffe, I., & Patterson, J. 2011, ApJS, 194, 28
Leach, R., Hessman, F. V., King, A. R., Stehle, R., & Mattei, J. 1999, MNRAS, 305, 225
Lomb, N. R. 1976, Ap&SS, 39, 447
Orosz, J. a., & Hauschildt, P. H. 2000, A&A, 364, 265
Patterson, J., Fenton, W. H., Thorstensen, J. R., et al. 2002, PASP, 114, 1364
Pecaut, M. J., & Mamajek, E. E. 2013, ApJS, 208, 9
Ritter, H., & Kolb, U. 2003, A&A, 404, 301
Rodríguez-Gil, P., Casares, J., Martínez-Pais, I. G., Hakala, P., & Steeghs, D. 2001, ApJL, 548, L49
Rodríguez-Gil, P., Gansicke, B. T., Hagen, H.-J., et al. 2007, MNRAS, 377, 1747
Rodríguez-Gil, P., Shahbaz, T., Marsh, T. R., et al. 2015, MNRAS, 452, 146
Sanchez-Blazquez, P., Peletier, R. F., Jimenez-Vicente, J., et al. 2006, MNRAS, 371, 703
Scargle, J. 1982, ApJ, 263, 835
Schlafly, E. F., & Finkbeiner, D. P. 2011, ApJ, 737, 103
Steiner, J., & Diaz, M. 1998, PASP, 110, 276
Stellingwerf, R. 1978, ApJ, 224, 953
Thorstensen, J. R., Ringwald, F. A., Wade, R. A., Schmidt, G. D., & Norsworthy, J. E. 1991, AJ, 102, 272
Warner, B. 1995, in Cataclysmic Variable Stars, ed. A. King et al. (Cambridge: Cambridge Univ. Press), 27